CHEMICAL PHYSICS

Direct tracking of ultrafast proton transfer in water dimers

Kirsten Schnorr[1,2]*, Michal Belina[3], Sven Augustin[1,2], Hannes Lindenblatt[1], Yifan Liu[1], Severin Meister[1], Thomas Pfeifer[1], Georg Schmid[1], Rolf Treusch[4], Florian Trost[1], Petr Slavíček[3]*, Robert Moshammer[1]

Upon ionization, water forms a highly acidic radical cation $H_2O^{+\cdot}$ that undergoes ultrafast proton transfer (PT)—a pivotal step in water radiation chemistry, initiating the production of reactive H_3O^+, $OH^\cdot$ radicals, and a (hydrated) electron. Until recently, the time scales, mechanisms, and state-dependent reactivity of ultrafast PT could not be directly traced. Here, we investigate PT in water dimers using time-resolved ion coincidence spectroscopy applying a free-electron laser. An extreme ultraviolet (XUV) pump photon initiates PT, and only dimers that have undergone PT at the instance of the ionizing XUV probe photon result in distinct $H_3O^+ + OH^+$ pairs. By tracking the delay-dependent yield and kinetic energy release of these ion pairs, we measure a PT time of (55 ± 20) femtoseconds and image the geometrical rearrangement of the dimer cations during and after PT. Our direct measurement shows good agreement with nonadiabatic dynamics simulations for the initial PT and allows us to benchmark nonadiabatic theory.

INTRODUCTION

Radiation chemistry is, to a large extent, the physics of ionizing radiation acting on water: Water is ubiquitous in living organisms, and most of the radiation-induced changes proceed indirectly via the formation of reactive intermediates in water. Understanding the action of ionizing radiation on water is, thus, a necessary prerequisite for a variety of applications ranging from medical radiation therapy to nuclear reactor technologies (*1*).

It is generally agreed that, upon valence ionization of solvated water molecules, proton transfer (PT) takes place, producing a hydronium ion (H_3O^+), a hydroxyl radical ($OH^\cdot$), and a (hydrated) electron

$$H_2O\cdots H_2O \xrightarrow[-e^-]{h\nu} H_2O\cdots H_2O^{+\cdot} \rightarrow H_3O^+\cdots OH^\cdot \rightarrow H_3O^+ + OH^\cdot$$

While the secondary reactions of these three highly reactive products have been studied in depth, details on the initial ultrafast PT step are still elusive. In particular, the PT time and its dependence on the initially excited electronic state and the geometrical rearrangement during and after PT have almost exclusively been subject to calculations. Measurements are complicated by the very fast nature of PT and the need to overcome the ionization potential of water to trigger PT. With the wider availability of short wavelength free-electron laser (FEL) sources, it starts to become possible to trace PT directly.

Early attempts to directly follow the PT in liquid water via broadband absorption spectroscopy could only place an upper limit on the PT time because they were hampered by the temporal resolution of the experimental apparatus (*2*). In a more recent soft x-ray transient absorption experiment, the PT time in liquid water was determined to be (46 ± 10) fs (*3*). While absorption spectroscopy gives insights into electronic structure changes, it does not allow one to follow the nuclear structure evolution of the intermediate and final cation structures directly. The formation time of the $(H_3O^+)OH$ complex in liquid water was recently determined to be 140 fs using time-resolved electron diffraction (*4*). Both successful experiments on the PT dynamics in liquid water used strong-field excitation pulses to overcome the ionization energy (IE) of water via multiphoton ionization. However, the interaction with a strong laser field perturbs the molecular potential, which may, in turn, alter the PT dynamics. Furthermore, it leaves the molecule ensemble in a rather undefined broadly excited state. Excitation with a single photon is a complementary and cleaner approach to trigger PT but experimentally more difficult due to the need to control laser pulses in the extreme ultraviolet (XUV) regime. Efforts with more state-specific excitation pulses are also ongoing using table-top laser sources (*5*, *6*).

Exploring the ionization dynamics in water clusters offers an appealing complementary alternative to the liquid phase to isolate and focus on the fundamental PT process. The molecular fragments can then be directly detected, and the dynamics can be investigated simultaneously in the time and energy domains. Water clusters provide a test bed for experiments [e.g., (*6*–*9*)] and theory [e.g., (*10*–*13*)] to study the photoionization and, in turn, PT dynamics of water in unprecedented detail for different target size (*14*). PT manifests as the almost exclusive formation of protonated water clusters following valence ionization, which was experimentally confirmed in clusters of various sizes using time-of-flight measurements (*15*–*17*). The smallest possible cluster, the water dimer, plays a prominent role: Calculations for the dimer can be performed most accurately and may, therefore, serve as asymptotic benchmarks for theories that aim at describing larger clusters and liquids (*10*, *11*, *18*). Furthermore, experiments can be unambiguously interpreted

[1]Max Planck Institute for Nuclear Physics, Saupfercheckweg 1, 69117 Heidelberg, Germany. [2]Paul Scherrer Institut, Forschungsstrasse 111, 5232 Villigen, Switzerland. [3]Department of Physical Chemistry, University of Chemistry and Technology, Technická 5, 16628 Prague 6, Czech Republic. [4]Deutsches Elektronen-Synchrotron DESY, Notkestr. 85, 22607 Hamburg, Germany.
*Corresponding author. Email: kirsten.schnorr@psi.ch (K.S.); petr.slavicek@vscht.cz (P.S.)

by directly tracing the composition of the products and their energies, which provides a more detailed view of the dynamics.

Here, we use time-resolved ion coincidence spectroscopy to track PT in water dimers using a single XUV photon from the pump pulse to induce PT and a single XUV photon from the probe pulse to track PT (cf. Fig. 1). In coincidence spectroscopy, we use momentum conservation to select only those ions that formed one dimer. Thus, it allows us to extract even rare reaction channels in small molecular clusters and their energetics by calculating their released kinetic energy after Coulomb explosion into ionic fragments (*19*, *20*). We exploit this unique advantage of following the dynamics in isolated water dimer cations by monitoring all created radical pairs ($H_3O^+\cdots OH^\cdot$ and $H_2O^{+\cdot}\cdots H_2O$) in real time, yielding a PT time of (55 ± 20) fs. Furthermore, by measuring the delay-dependent kinetic energy release (KER) of the ionic fragments, we are able to draw conclusions on the intermolecular geometry changes during and after PT. Our nonadiabatic dynamics calculations show an overall very good agreement with the experimental results. We demonstrate that gas-phase ion coincidence spectroscopy enables tracking PT in dimers directly and to follow the associated geometrical changes. The present experiment allows us to benchmark theory and might open up the possibility to unravel even more complex ultrafast processes in water radiation chemistry.

RESULTS

The experimental scheme that we used to determine the PT time in water dimers is illustrated in Fig. 1. We use two identical XUV pulses with adjustable delay to perform an XUV-pump–XUV-probe experiment. One photon from the pump pulse ionizes one water molecule. The selected photon energy of 24 eV is sufficient to remove an electron from one of the three lowest electronic states in a water molecule with the IEs: IE($1b_1$) = 12.6 eV, IE($3a_1$) = 14.8 eV, and IE($1b_2$) = 18.6 eV [the binding energies of water dimers are similar, e.g., for the highest occupied molecular orbital (HOMO) level, the ($1b_1$) peak splits into two peaks at 12.1 and 13.2 eV; (*21*)]. Ionization of all three states occurs with similar probability due to their similar cross sections σ: σ($1b_1$) = 6.5 Mb, σ($3a_1$) = 5.8 Mb, and σ($1b_2$) = 6.5 Mb (*22*). According to calculations and previous experiments, the majority of valence-ionized water dimers is expected to undergo PT.

In our experiment, the onset of PT is probed by further ionizing the generated dimer cation with the probe pulse (cf. Fig. 1). Only if PT is completed at the instance of the probe pulse, $H_3O^+ + OH^+$ ion pairs are created and detected. To exclude the production of doubly charged H_3O^{2+} ions, the photon energy was chosen below the IE of the singly charged H_3O^+ cation (*23*); see also the Supplementary Materials. In contrast, if PT is not completed when the probe pulse further ionizes, then $H_2O^+ + H_2O^+$ ion pairs are produced. Therefore, the signature of PT is imprinted in both the delay-dependent yield of $H_3O^+ + OH^+$ and $H_2O^+ + H_2O^+$ ion pairs. Using ion coincidence spectroscopy (*20*), we have measured the delay-dependent ion yield and KER of both respective reaction pathways. We assume that, in the second ionization step, all outer valence electrons can be ionized from the neutral particle, which can be either H_2O or the $OH^\cdot$ radical. This is confirmed by our calculations.

The delay-dependent yield of coincident $H_3O^+ + OH^+$ ion pairs, shown in Fig. 2A, increases for larger delays due to more cations undergoing PT and provides clear evidence that PT is taking place. In contrast, the $H_2O^+ + H_2O^+$ coincidence channel in Fig. 2B shows the anticipated decreased rate for large delays. Both delay-dependent yields are riding on a constant background, which stems from a combination of false coincidences and two-photon absorption within the pump or the probe pulse alone (see details in the Supplementary Materials). For the $H_2O^+ + H_2O^+$ coincidence channel, two-photon absorption within one pulse is the by far dominating process. Furthermore, a narrow peak appears at time zero, which we attribute to an enhanced intensity and, in turn, multiphoton rate due to temporally overlapping coherent self-amplified spontaneous emission (SASE) spikes (*24*) of the pump and the probe pulses. Competing relaxation channels from highly excited electronic states, which result in water cation fragments, are also present (*18*). In summary, the $H_2O^+ + H_2O^+$ channel is strongly contaminated by multiphoton ionization manifesting as a constant background as well as a rate increase at time zero and competing decay channels. In contrast, the only mechanism resulting in $H_3O^+ + OH^+$ ion pairs is PT. Thus, we use it to extract the PT time.

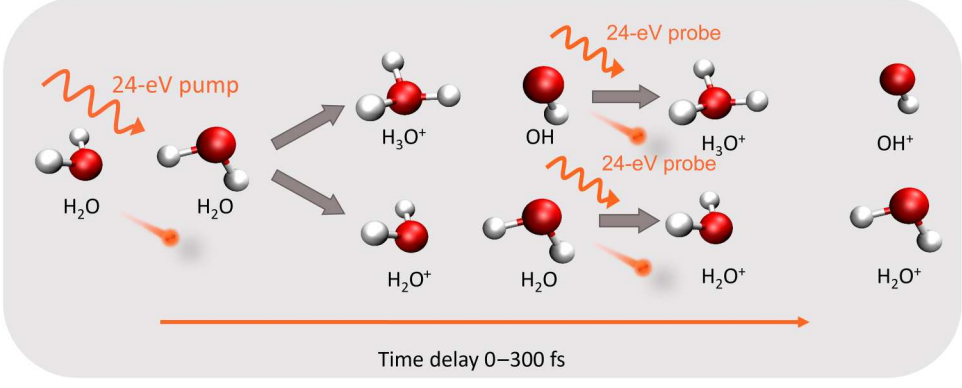

Fig. 1. Pump-probe scheme used to investigate the PT dynamics in water dimers. Triggered by valence ionization through absorption of a 24-eV pump photon, water dimer cations may either undergo PT resulting in $H_3O^+\cdots OH$ complexes or remain $(H_2O\cdots H_2O)^+$ complexes. The probe pulse, which is delayed up to 300 fs, further ionizes one of the neutral species. Because $H_3O^+ + OH^+$ ion pairs can only be generated if PT is completed by the time that the probe pulse arrives, this reaction channel provides a clean signature to track PT. If PT is not completed when the probe pulse further ionizes, then $H_2O^+ + H_2O^+$ ion pairs are produced and detected.

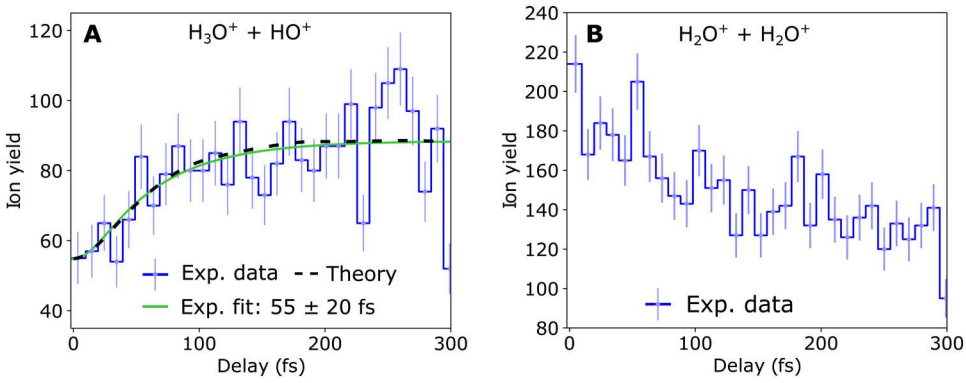

Fig. 2. Measured delay-dependent ion yields. (**A**) The measured delay-dependent ion yield for coincident H_3O^+ + OH^+ ion pairs is shown in blue with light blue error bars (statistical counting error). An exponential fit convoluted with the pulse duration plotted in green yields a PT time constant of (55 ± 20) fs. The calculated state-averaged delay-dependent ion yield is plotted as black dashed line. The displayed simulated data were convoluted with the measured pulse duration and scaled and offset with the parameters from the exponential fit (green) of the experimental data. The simulated state-averaged PT time amounts to 60 fs when fitted with an exponential. (**B**) The measured delay-dependent ion yield for coincident H_2O^+ + H_2O^+ ion pairs is shown in blue with light blue error bars (statistical counting error).

To determine the PT time, the delay-dependent H_3O^+ + OH^+ ion yield is fitted with an exponential rise convoluted with the FEL pulse duration of 40 fs (Fig. 2A), yielding a rise time of (55 ± 20) fs. The error bars correspond to 1 standard deviation. The experimental observation time window of 300 fs limits the accessible lifetimes and omits the observation of possible slow decay channels on the hundreds of femtosecond time scales. The corresponding calculated state-averaged H_3O^+ + OH^+ ion yield, convoluted with the measured pulse duration and offset and scaled with the results of the exponential fit of the experimental data, is shown as a black dashed line in Fig. 2A. Fitting the rise time of the simulated ion yield with an exponential function $[1 - \exp(-t/\tau)]$results in a PT time of 60 fs. The averaged calculated and measured H_3O^+ + OH^+ ion yields in Fig. 2A show an excellent agreement. A more detailed view of the reactions initiated by valence ionization is provided in Fig. 3, where the ratios of the different product channels are analyzed. The ionization into the D_0 state leads almost exclusively to PT, and the H_3O^+···OH complex stays bound within the simulation period. Ionizing the higher states leads to a higher degree of fragmentation. For $1b_2$ ionization, three-body fragmentation is even dominant. Therefore, the lower-lying electronic states contribute more to the H_3O^+ + OH^+ channels.

The summed kinetic energy of all ionic fragments (KER) allows us to draw conclusions on the dynamical changes of internuclear distances because it is inversely proportional to the cations' intermolecular distance R, not considering molecular bonds: KER $\sim \frac{1}{R}$. This holds only approximately, as we show in the Supplementary Materials. The measured and simulated KER distributions for several time delays averaged over all electronic states resulting in H_3O^+ + OH^+ and H_2O^+ + H_2O^+ ion pairs are shown in Fig. 4 (A to D). The measured KERs for early (25 to 75 fs) and late (225 to 275 fs) delays are shown in blue and red, respectively, in Fig. 4 (A and B) for both ion yield channels. The simulated KERs in Fig. 4 (C and D) are displayed for three delay points 50, 100, and 250 fs. Notably, the contribution of ion pairs with KERs below 4 eV is increasing with the time delay. The origin of these low KERs can be understood with the help of the delay-dependent KER spectra, shown in Fig. 5 (A to D).

The measured delay-dependent KER distribution of H_3O^+ + OH^+ ion pairs in Fig. 5A contains contributions with different KER time dependencies. For small delays, the KER distribution is narrow and centered around 4.5 eV. Toward larger delays, the distribution is drawn out to smaller energies with a continuous KER distribution reaching down to 2 eV. Ion pairs with a decreasing KER for larger delays undergo dissociation during the delay between pump and probe pulse. Thus, they are ionized by the probe pulse at a larger R, resulting in smaller KERs. In contrast, ion pairs with a constant KER for all delays have not undergone dissociation or another intermolecular rearrangement up to our largest measured delay of 300 fs. These cations are either stable or have substantially longer dissociation times than the observation time window. Consequently, nondissociating H_3O^+···OH structures have a constant KER around 4.5 eV, and dissociating H_3O^+···OH ion pairs exhibit a broad delay-dependent KER distribution. The amount of dissociating structures, which fan out to low KERs, is well reproduced with the theoretical simulations at the extended multi-state complete active space perturbation theory n=2 (XMS-CASPT2) level (cf. Fig. 5C). The XMS-CASPT2 can be contrasted with the complete active space self-consistent field (CASSCF) calculations, lacking the dynamical correlation; see the Supplementary Materials. These calculations predict a faster dissociation time than measured in the experiment.

The simulated delay-dependent H_2O^+ + H_2O^+ KER distribution (see Figs. 5D and 4D) peaks around 50 fs, rising to KERs beyond 5 eV, and decreases afterward. In the corresponding experimental data (Fig. 5B), this KER increase is not visible. The KER increase around 50 fs in theory indicates that the intermolecular distance decreases when PT takes place. Furthermore, the calculated delay-dependent H_2O^+ + H_2O^+ KER distribution in Fig. 5D shows almost no ion pairs for large delays, which is expected due to the fast PT time constant. A fraction of the KER distribution branches out to lower values with growing delay, which indicates H_2O^+···H_2O cations that dissociate or start to dissociate within 300 fs. The amount of nondissociating ion pairs is similar (cf. Fig. 4D). In contrast, the measured delay-dependent H_2O^+ + H_2O^+ KER distribution, shown in Fig. 5B, is dominated by a constant KER distribution centered around 4.3 eV for all delays. While the expected ion yield drop

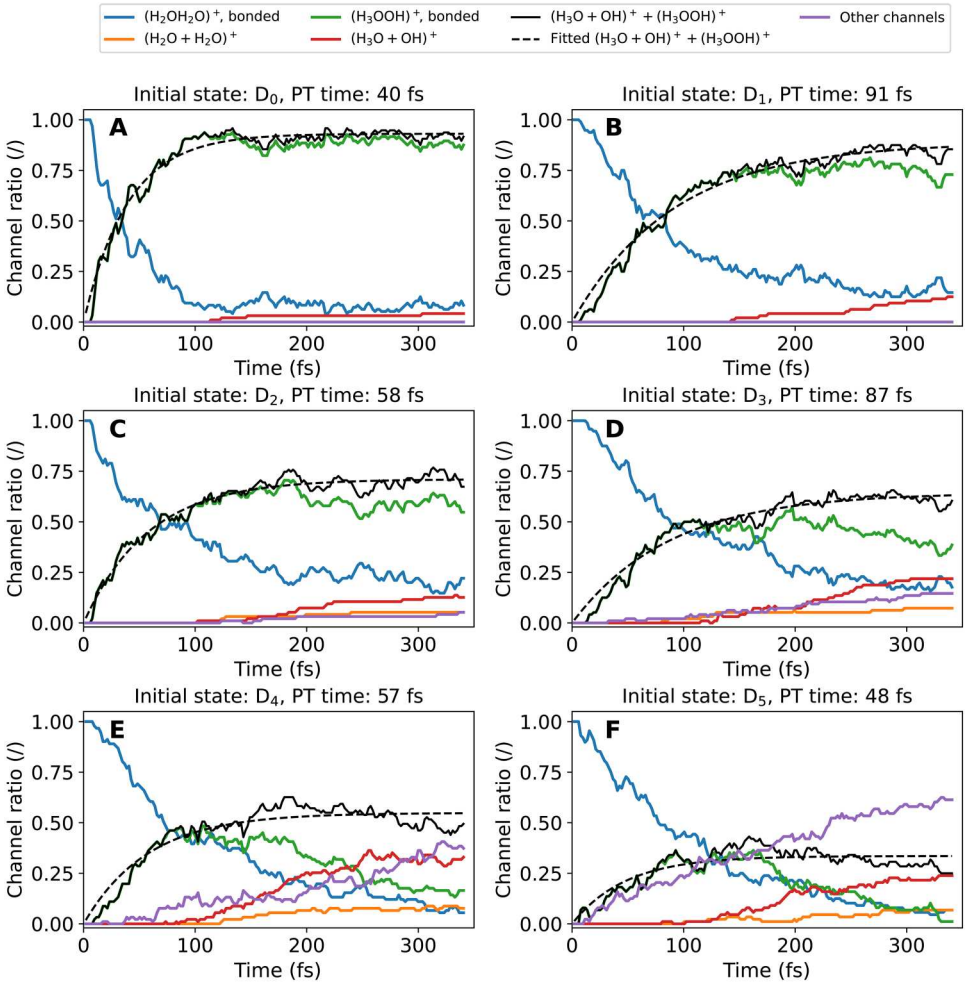

Fig. 3. Calculated reaction yields for different reaction channels. The reaction yield curves are different for each of the electronic states, which is specified above in each of the subplots [Subplots (**A**) to (**F**) show the NAMD starting from the D_1-D_6 states, respectively]. The full black curve represents the summation of both PT channels, and the dotted black curve is the fitted exponential function of the summation. Individual fitted PT times are indicated at the top of each subplot. The calculations were performed at the XMS-CASPT2 level. See also the Supplementary Materials for a detailed list of other channels.

with increasing delay is clearly visible, the majority of the signal remains for large delays (cf. Fig. 4B). This background can be attributed to two-photon absorption within one pulse, which creates ion pairs with constant KERs for all delays. In particular, for large delays, when most dimer cations have completed PT, the signal is dominated by multiphoton ionization. Thus, the experiment does not allow us to draw clear conclusions on the structural evolution of $H_2O\cdots H_2O^+$ complexes on longer time scales because the multiphoton signal and the pump-probe signal can not be disentangled.

Multiphoton ionization resulting in $H_2O^+ + H_2O^+$ ion pairs does, however, allow us to retrieve the dimer cation structure just after excitation (i.e., the ground state structure) by applying the so-called reflection principle (*25*–*27*). Such an approach offers a simulation-free method to determine the structure of the clusters, and it is, therefore, interesting to see the applicability of this approach for multidimensional systems. Figure 6 shows the evaluated nuclear density along the O-O coordinate together with a calculated distribution from the path integral–based simulations. As the simulated KER for the smallest delay in Fig. 4D agrees well with the corresponding experimental KER in Fig. 4B, we can assume that these distributions are close to the real situation. However, when we would assume only the Coulomb forces between the water molecules, the calculated and reflection-principle distributions differ quite a lot. The agreement gets very good once we take into account also the polarization forces. The simulated and reflection-principle maxima almost coincide, yet the distribution extracted from the KER is broader than the molecular dynamics (MD) model. Note that the calculations cover both the thermal motion and nuclear quantum effects, including anharmonicities. Thus, the discrepancy most likely stems from the reduction of the multidimensional problem to a single dimension defined by a single coordinate *R*. The broader experimental peak could partially also stem from the dissociation on different dicationic states than used in the calculations; however, the different states are largely parallel. A more detailed analysis is provided in the Supplementary Materials; see also fig. S16.

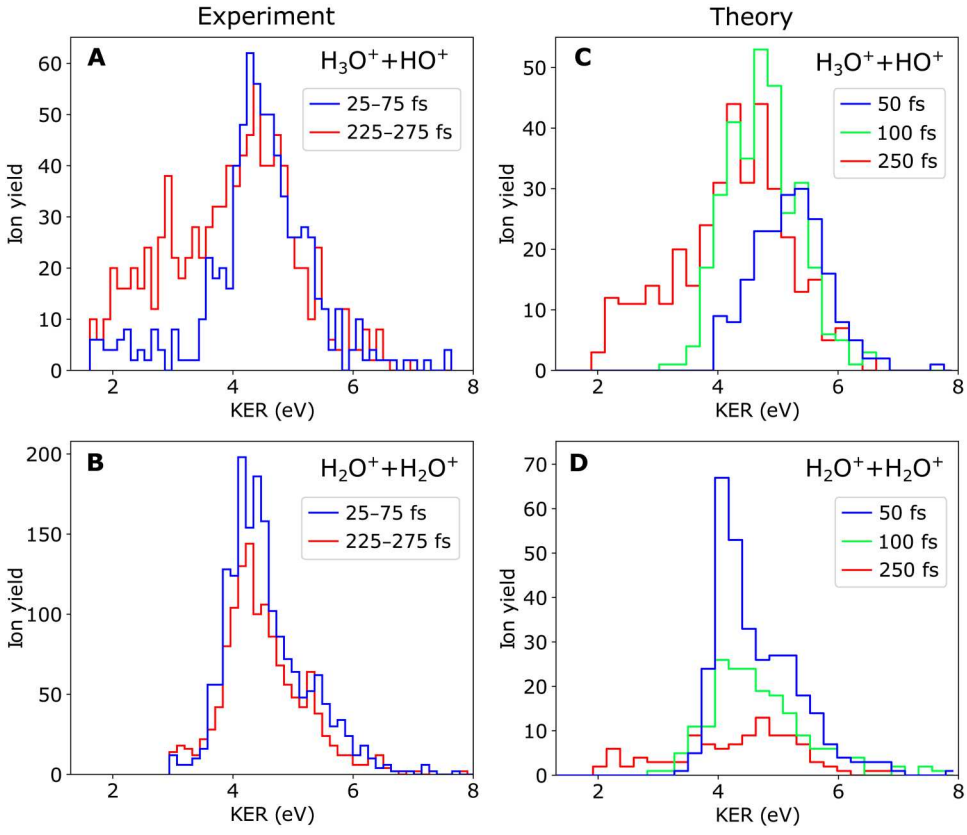

Fig. 4. Measured and calculated KER distributions for different delays and ion channels. Measured KER for coincident (**A**) $H_3O^+ + OH^+$ and (**B**) $H_2O^+ + H_2O^+$ ion pairs for early delays (25 to 75 fs) in blue and late delays (225 to 275 fs) in red. The corresponding simulated KERs for (**C**) $H_3O^+ + OH^+$ and (**D**) $H_2O^+ + H_2O^+$ ion pairs are plotted at 50 fs in blue, at 100 fs in green, and at 250 fs in red. The *y* axes are ion yields, where absolute comparisons are only possible within a theory or experiment plot.

DISCUSSION

Time-resolved coincident ion momentum spectroscopy provided us with a clear picture of the dynamical processes following the valence ionization of water dimers. The dominant process is PT, taking place in (55 ± 20) fs. Within the first 300 fs, there is very limited nuclear motion of the oxygen atoms in the dimer.

The combined experimental difficulty of PT being a fast process on the few tens of femtosecond time scale and being only accessible by a single photon in the VUV (vacuum ultraviolet) or XUV regime poses high demands on the pump and probe pulses for such a measurement in the single-photon absorption regime. Efforts in this direction are ongoing: In a pioneering experiment on small water clusters, sub–50-fs VUV pulses were used for resonant excitation of the water molecules, and subsequent hydrogen transfer was probed with an 800-nm strong-field pulse (*5*). In a more recent time-resolved experiment on larger water clusters, a single-photon excitation scheme was used to study the formation time of the solvated electron applying VUV pulses from low-order harmonic generation (*6*). In our experiment, the unique properties of an XUV FEL are exploited to generate two intrinsically synchronized XUV pulses for single ionization within the pump and single ionization within the probe pulse. The detection of $H_3O^+ + OH^+$ ion pairs is an unmistakable signature of PT, which is also validated by theory. With this information, our experiment is able to benchmark calculations of the PT lifetime and the dimer cation dynamics after ionization. Because the used photon energy of 24 eV is well beyond the IE of water, we also gain access to the PT dynamics of higher excited states, which are predicted to proceed differently (*18*, *28*). While we measure a state-averaged PT time and dynamics, coincident detection of photoelectrons would allow one to extract details of the PT time and nuclear rearrangement following the removal of electrons from individual electronic states.

In a previous ion coincidence experiment on water dimers, where a single strong-field 800-nm laser pulse was used to double ionize the dimers, the measured yield of $H_3O^+ + OH^+$ ion pairs was found to be consistent with a PT time of ~30 fs (*8*). The difference to our result is relatively small, especially considering error bars in both experiments. The measurements are, however, quite different: On the one hand, strong-field laser excitation populates a broad range of excited states, and only a fraction of the molecules ends up ionized. On the other hand, a strong-field pulse influences the molecular potentials and may, in turn, affect the PT dynamics, which is a particular concern in a fragile system, like the water dimer. The latter is generally unknown in any experiment where multiphoton excitation or ionization is applied. Other recent experiments looking into the PT dynamics in liquid water (*3*, *4*) also used strong-field pump pulses and, therefore, suffer the same uncertainties.

The present experiments can be used for benchmarking the dynamical calculations. Therefore, we would like to point out which levels of theory we found to be necessary for quantitative modeling of the water dimer ionization: First, we need to correctly sample the

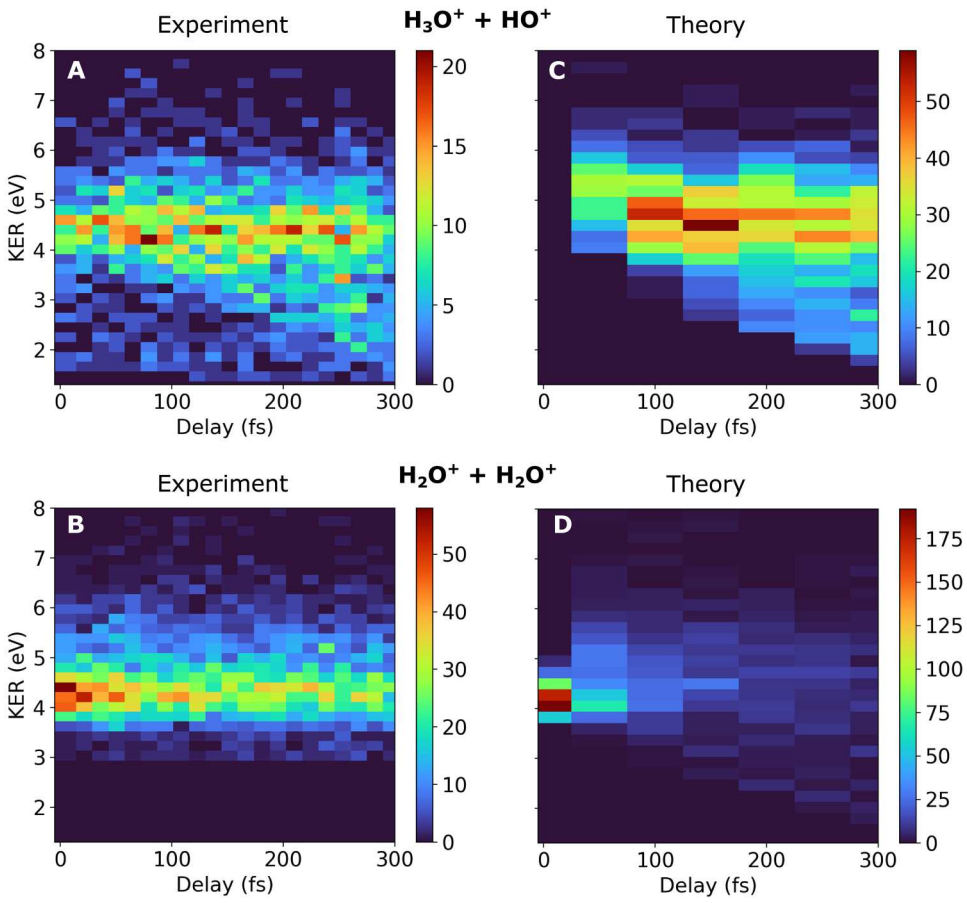

Fig. 5. Measured and calculated delay-dependent KER distributions for different ion channels. Measured (**A** and **B**) and state-averaged simulated (**C** and **D**) delay-dependent KER distributions of $H_3O^+ + OH^+$ and $H_2O^+ + H_2O^+$ ion pairs.

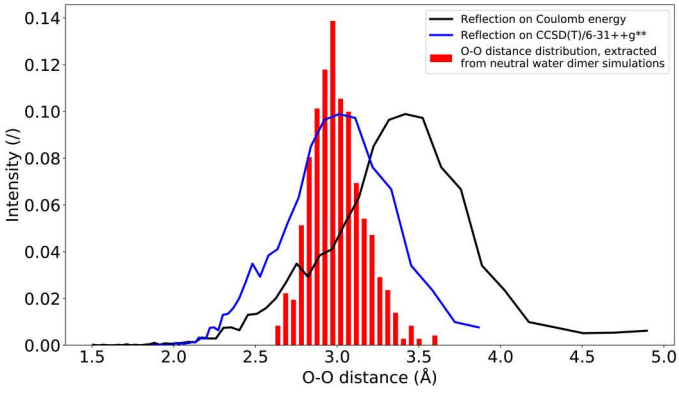

Fig. 6. Reflection-principle estimate of the O-O distance distribution in neutral water dimers. The bars show the results of the simulation based on the generalized Langevin equation (GLE), using the BMK/6-31++g** theory for describing the electronic structure. The black curve shows the distribution extracted from the measured KER, considering only Coulomb interaction between the two charged water units. The blue curve shows the distribution extracted with the calculated ab initio intermolecular potential for the triplet ground state of the dication; see also fig. S16 more details.

initial conditions, taking into account both the thermal motion and nuclear quantum effects as well as including the anharmonicities. This can be done with path integral simulations or using the quantum thermostat approach. Second, nonadiabatic simulations are needed to describe dynamics starting at different interacting electronic states. It turns out that these different states contribute quite distinctly to the observed reaction channels, i.e., $H_3O^+ + OH^+$ and $H_2O^+ + H_2O^+$. Last, we emphasize the role of the electronic structure description: Multireference treatment is needed to account for all the interacting states. However, the dynamical correlation is also important to achieve a quantitative agreement. While the dynamics with both applied methods, CASSCF and XMS-CASPT2, predict the ultrafast PT correctly, only the latter method is able to also predict the long stability of the formed complexes.

Most of the previous theoretical studies focused dominantly on the ground state dynamics of the ions, e.g., (*29*–*33*). Other studies focused on water complexes ionized by strong-field ionization (*34*). Water dimer dynamics for the HOMO ionization using wave packet simulations on a reduced dimensionality potential energy surface at the equation-of-motion ionization-potential coupled-cluster singles and doubles (EOM-IP-CCSD) level have also been studied (*28*). These simulations have already pointed to some differences between the lowest ionized state and the lowest excited cationic state at the very short time scales before the nonadiabatic effects

started to play a role. The differences for all valence electronic states were also observed in CASSCF dynamics (*35*).

Our study demonstrates the capability and great potential to probe molecular dynamics of weakly bound systems using XUV/x-ray pump and probe pulses using an FEL source. Ionization at XUV/x-ray energies is typically perturbative in contrast to strong-field multiphoton interactions or streaking scenarios at long wavelengths. It lays the foundation for future experiments to investigate radiation chemistry using multiparticle coincidence spectroscopy exploiting the full potential of the upcoming high–repetition rate FEL facilities.

For water complexes, small molecular clusters are the upper size limit for time-resolved coincidence momentum spectroscopy as we need to record all outgoing fragments. While this method brings an unprecedented level of detail to chemical dynamics, one might ask whether the results are relevant for condensed matter, e.g., in the context of radiation chemistry. The water dimer is the smallest unit that allows us to track the elementary reactions in radiation chemistry like PT. The processes following upon PT already differ for the different phases: In the gas phase, the charged clusters dissociate, whereas, in liquid water, the charges separate via the Grotthuss mechanism. The dimer also has distinguishable hydrogen bond donor and hydrogen bond acceptor units; this separation is not seen anymore already for the trimer. However, our time- and energy-resolved data allow us to understand how much of the energy is deposited into electronic and internal degrees of freedom, which is the same also for the liquid phase. Ultimately, a full picture of PT can, thus, be only gained by combining complementary experiments from different phases. Furthermore, a water dimer is simple enough for chemical theory. Nonadiabatic on-the-fly simulations at high electronic structure levels such as those presented here or wave packet simulations are still possible. The presented data can, thus, serve as a basis for benchmarking of the nonadiabatic simulations in the condensed phase.

MATERIALS AND METHODS

Experiment

The experiment was carried out at the FLASH2 FEL in Hamburg using the Reaction Microscope endstation at FL26 (*36*, *37*). The FEL was tuned to a photon energy of 24 eV, yielding a pulse energy of 10 μJ and a pulse duration of ∼40 fs (full width at half maximum) at a repetition rate of 800 pulses/s. Identical XUV-pump–XUV-probe pulses with tuneable delay were produced using a multilayer-mirror split, delay and focusing setup. The delay was continuously scanned up to 300 fs with time zero as well as the pulse duration determined in an independent cross-correlation measurement on argon (cf. the Supplementary Materials) (*38*). The FEL beams were spatially overlapped in a supersonic water cluster jet, generated by a heatable nozzle with in-vacuum water reservoir. The dimer production rate was optimized to ∼1% using a water reservoir temperature of 44°C and—to avoid condensation—keeping the nozzle warmer at 70°C. Photoions were accelerated in a homogeneous electric field of 38 V cm^{-1} toward an microchannel plate (MCP)–delay line detector combination. Using the impact time and position, the three-dimensional momenta and KERs of the generated water dimer fragments were reconstructed (*19*, *20*). The KER for selected coincident ion pairs, i.e., $H_2O^+ + H_2O^+$ and $H_3O^+ + OH^+$, is analyzed as a function of the delay of the XUV pump-probe pulses. More details are given in the Supplementary Materials.

Theory

The ab initio simulations attempted to model the ultrafast reactions following the removal of electrons from outer valence orbitals. In the present study, we considered the ionization from the $1b_1$, $3a_1$, and $1b_2$ orbitals (six states in total). We have performed the simulations using the nonadiabatic surface hopping scheme in its fewest switches version (*39*). The electronic structure was described with the extended multistate complete active space second-order perturbation theory (XMS-CASPT2), which covers both the dynamical and static correlation. We used the correlation-consistent polarized valence-only double-zeta (cc-pVDZ) basis set. The energies, gradients, and nonadiabatic couplings were evaluated in the brilliantly advanced general electronic-structure library (BAGEL) electronic structure package, version 1.2.0 (*40*). The active space was set to 11 electrons in six orbitals for the singly ionized states. We have considered six states in the doublet manifold, corresponding to the ionization of both the proton donor and proton acceptor water molecules in their $1b_1$, $3a_1$, and $1b_2$ states. The equations of motion were integrated using the Verlet algorithm, with an integration time step set to 4 atomic units (a.u.), which correspond to approximately 0.1 fs. The total length of the simulations was 350 fs. The nonadiabatic simulations show a nonnegligible fraction of trajectories that have ended prematurely due to electronic structure problems (maximum of 7% for the initial state D_4). Only successfully finished trajectories were used for the analysis and further calculations. For comparison, we have also performed the dynamical calculations at the CASSCF level, lacking the dynamical part of correlation. These data are shown in the Supplementary Materials.

To decide what will be the final outcome of the pump-probe experiment, we have simulated the ensemble of structures for a given delay time in the doubly ionized state. These simulations were performed with the CASSCF method and the 6-31++g** basis set in the Molpro computational package, version 2012.1.11 (*41*). The active space was set to 10 electrons in six orbitals. Only the triplet ground state was considered during the calculations due to the better stability of these calculations. However, the energetics for the singlet and triplet manifold is comparable for the water dimer case; see fig. S16. The simulation step size was set to 4 a.u., and the total length was 97 fs.

The initial conditions for the water dimer in the neutral state were generated using molecular dynamics with the quantum thermostat based on the generalized Langevin equation (GLE) (*42*). In this way, the nuclear quantum effects are taken into account for both the atomic positions and momenta. This approach provides an exact mapping of the system onto the phase space for harmonic systems, yet, in our experience, it reliably describes also moderately anharmonic systems. The temperature was set to 180 K, and the GLE parameters $\hbar\omega/kT = 50$ and $Ns = 50$ were taken from the GLE4MD website (*43*). The time step for the GLE MD was 20 a.u. (approximately 0.48 fs), and the total simulation length was set to 20 ps. Energies and gradients were evaluated with the Boese-Martin for kinetics (BMK) functional (*44*) and 6-31++g** basis set using the Gaussian09 package, revision D.01 (*45*). All the dynamical calculations were performed in our in-house multipurpose ab initio MD program (ABIN) code (*35*).

Supplementary Materials

This PDF file includes:

Figs. S1 to S16
Tables S1 and S2
References

REFERENCES AND NOTES

1. B. C. Garrett, D. A. Dixon, D. M. Camaioni, D. M. Chipman, M. A. Johnson, C. D. Jonah, G. A. Kimmel, J. H. Miller, T. N. Rescigno, P. J. Rossky, S. S. Xantheas, S. D. Colson, A. H. Laufer, D. Ray, P. F. Barbara, D. M. Bartels, K. H. Becker, K. H. Bowen, S. E. Bradforth, I. Carmichael, J. V. Coe, L. R. Corrales, J. P. Cowin, M. Dupuis, K. B. Eisenthal, J. A. Franz, M. S. Gutowski, K. D. Jordan, B. D. Kay, J. A. LaVerne, S. V. Lymar, T. E. Madey, C. W. McCurdy, D. Meisel, S. Mukamel, A. R. Nilsson, T. M. Orlando, N. G. Petrik, S. M. Pimblott, J. R. Rustad, G. K. Schenter, S. J. Singer, A. Tokmakoff, L.-S. Wang, T. S. Zwier, Role of water in electron-initiated processes and radical chemistry: Issues and scientific advances. *Chem. Rev.* **105**, 355–390 (2005).
2. O. Marsalek, C. G. Elles, P. A. Pieniazek, E. Pluhařová, J. VandeVondele, S. E. Bradforth, P. Jungwirth, Chasing charge localization and chemical reactivity following photoionization in liquid water. *J. Chem. Phys.* **135**, 224510 (2011).
3. Z.-H. Loh, G. Doumy, C. Arnold, L. Kjellsson, S. H. Southworth, A. Al Haddad, Y. Kumagai, M.-F. Tu, P. J. Ho, A. M. March, R. D. Schaller, M. S. Bin Mohd Yusof, T. Debnath, M. Simon, R. Welsch, L. Inhester, K. Khalili, K. Nanda, A. I. Krylov, S. Moeller, G. Coslovich, J. Koralek, M. P. Minitti, W. F. Schlotter, J.-E. Rubensson, R. Santra, L. Young, Observation of the fastest chemical processes in the radiolysis of water. *Science* **367**, 179–182 (2020).
4. M.-F. Lin, N. Singh, S. Liang, M. Mo, J. P. F. Nunes, K. Ledbetter, J. Yang, M. Kozina, S. Weathersby, X. Shen, A. A. Cordones, T. J. A. Wolf, C. D. Pemmaraju, M. Ihme, X. J. Wang, Imaging the short-lived hydroxyl-hydronium pair in ionized liquid water. *Science* **374**, 92–95 (2021).
5. H. T. Liu, J. P. Müller, M. Beutler, M. Ghotbi, F. Noack, W. Radloff, N. Zhavoronkov, C. P. Schulz, I. V. Hertel, Ultrafast photo-excitation dynamics in isolated, neutral water clusters. *J. Chem. Phys.* **134**, 094305 (2011).
6. V. Svoboda, R. Michiels, A. C. LaForge, J. Med, F. Stienkemeier, P. Slavíček, H. J. Wörner, Real-time observation of water radiolysis and hydrated electron formation induced by extreme-ultraviolet pulses. *Sci. Adv.* **6**, eaaz0385 (2020).
7. S. Barth, M. Ončk, V. Ulrich, M. Mucke, T. Lischke, P. Slavíček, U. Hergenhahn, Valence ionization of water clusters: From isolated molecules to bulk. *J. Phys. Chem. A* **113**, 13519–13527 (2009).
8. C. Zhang, J. Lu, T. Feng, H. Rottke, Proton transfer dynamics following strong-field ionization of the water dimer. *Phys. Rev. A* **99**, 053408 (2019).
9. C. Richter, D. Hollas, C. M. Saak, M. Förstel, T. Miteva, M. Mucke, O. Björneholm, N. Sisourat, P. Slavíček, U. Hergenhahn, Competition between proton transfer and intermolecular Coulombic decay in water. *Nat. Commun.* **9**, 4988 (2018).
10. S. Tomoda, K. Kimura, Proton-transfer potential-energy surfaces of the water dimer cation $(H_2O)_2^+$ in the $1^2A''$ and $1^2A'$ states. *J. Chem. Phys.* **82**, 215–227 (1983).
11. R. N. Barnett, U. Landman, Pathways and dynamics of dissociation of ionized $(H_2O)_2$. *J. Phys. Chem.* **99**, 17305–17310 (1995).
12. H. Tachikawa, Ionization dynamics of the small-sized water clusters: A direct ab initio trajectory study. *J. Phys. Chem. A* **108**, 7853–7862 (2004).
13. J. D. Herr, J. Talbot, R. P. Steele, Structural progression in clusters of ionized water, $(H_2O)^+_{n=1-5}$. *J. Phys. Chem. A* **119**, 752–766 (2015).
14. D. Mi, K. Chingin, Water radical cations in the gas phase: Methods and mechanisms of formation, structure and chemical properties. *Molecules* **25**, 3490 (2020).
15. P. P. Radi, P. Beaud, D. Franzke, H.-M. Frey, T. Gerber, B. Mischler, A.-P. Tzannis, Femtosecond photoionization of $(H_2O)_n$ and $(D_2O)_n$ clusters. *J. Chem. Phys.* **111**, 512–518 (1999).
16. F. Dong, S. Heinbuch, J. J. Rocca, E. R. Bernstein, Dynamics and fragmentation of van der Waals clusters: $(H_2O)_n$, $(CH_3OH)_n$, and $(NH_3)_n$ upon ionization by a 26.5eV soft x-ray laser. *J. Chem. Phys.* **124**, 224319 (2006).
17. H. Shiromaru, H. Shinohara, N. Washida, H.-S. Yoo, K. Kimura, Synchrotron radiation measurements of appearance potentials for $(H_2O)_2^+$, $(H_2O)_3^+$, $(H_2O)_2H^+$ and $(H_2O)_3H^+$ in supersonic jets. *Chem. Phys. Lett.* **141**, 7–11 (1987).
18. O. Svoboda, D. Hollas, M. Oncak, P. Slavíček, Reaction selectivity in an ionized water dimer: Nonadiabatic ab initio dynamics simulations. *Phys. Chem. Chem. Phys.* **15**, 11531–11542 (2013).
19. R. Dörner, V. Mergel, O. Jagutzki, L. Spielberger, J. Ullrich, R. Moshammer, H. Schmidt-Böcking, Cold target recoil ion momentum spectroscopy: A 'momentum microscope' to view atomic collision dynamics. *Phys. Rep.* **330**, 95–192 (2000).
20. J. Ullrich, R. Moshammer, A. Dorn, R. Dörner, L. P. H. Schmidt, H. Schmidt-Böcking, Recoil-ion and electron momentum spectroscopy: Reaction-microscopes. *Rep. Prog. Phys.* **66**, 1463–1545 (2003).
21. S. Tomoda, Y. Achiba, K. Kimura, Photoelectron spectrum of the water dimer. *Chem. Phys. Lett.* **87**, 197–200 (1982).
22. J. W. Gallagher, C. E. Brion, J. A. R. Samson, P. W. Langhoff, Absolute cross sections for molecular photoabsorption, partial photoionization, and ionic photofragmentation processes. *J. Phys. Chem. Ref. Data Monogr.* **17**, 9–153 (1988).
23. C. Domesle, S. Dziarzhytski, N. Guerassimova, L. S. Harbo, O. Heber, L. Lammich, B. Jordon-Thaden, R. Treusch, A. Wolf, H. B. Pedersen, Photoionization and fragmentation of H_3O^+ under XUV irradiation. *Phys. Rev. A* **88**, 043405 (2013).
24. T. Pfeifer, Y. Jiang, S. Düsterer, R. Moshammer, J. Ullrich, Partial-coherence method to model experimental free-electron laser pulse statistics. *Opt. Lett.* **35**, 3441–3443 (2010).
25. W. Scott Hopkins, S. R. MacKenzie, Communication: Imaging wavefunctions in dissociative photoionization. *J. Chem. Phys.* **135**, 081104 (2011).
26. L. P. H. Schmidt, T. Jahnke, A. Czasch, M. Schöffler, H. Schmidt-Böcking, R. Dörner, Spatial imaging of the H_2^+ vibrational wave function at the quantum limit. *Phys. Rev. Lett.* **108**, 073202 (2012).
27. S. Zeller, M. Kunitski, J. Voigtsberger, A. Kalinin, A. Schottelius, C. Schober, M. Waitz, H. Sann, A. Hartung, T. Bauer, M. Pitzer, F. Trinter, C. Goihl, C. Janke, M. Richter, G. Kastirke, M. Weller, A. Czasch, M. Kitzler, M. Braune, R. E. Grisenti, W. Schöllkopf, L. P. H. Schmidt, M. S. Schöffler, J. B. Williams, T. Jahnke, R. Dörner, Imaging the He_2 quantum halo state using a free electron laser. *Proc. Natl. Acad. Sci. U.S.A.* **113**, 14651–14655 (2016).
28. E. Kamarchik, O. Kostko, J. M. Bowman, M. Ahmed, A. I. Krylov, Spectroscopic signatures of proton transfer dynamics in the water dimer cation. *J. Chem. Phys.* **132**, 194311 (2010).
29. H. Tachikawa, Ionization dynamics of a water dimer: Specific reaction selectivity. *Phys. Chem. Chem. Phys.* **13**, 11206–11212 (2011).
30. H. M. Lee, K. S. Kim, Dynamics and structural changes of small water clusters on ionization. *J. Comput. Chem.* **34**, 1589–1597 (2013).
31. H. Tachikawa, T. Takada, Proton transfer rates in ionized water clusters $(H_2O)_n$ (n = 2–4). *RSC Adv.* **5**, 6945–6953 (2015).
32. D. M. Chipman, Hemibonding between water cation and water. *J. Phys. Chem. A* **120**, 9618–9624 (2016).
33. J. Chalabala, F. Uhlig, P. Slavíček, Assessment of real-time time-dependent density functional theory (RT-TDDFT) in radiation chemistry: Ionized water dimer. *J. Phys. Chem. A* **122**, 3227–3237 (2018).
34. Z. P. Wang, P. M. Dinh, P. G. Reinhard, E. Suraud, Ultrafast nonadiabatic dynamics of a water dimer in femtosecond laser pulses. *Laser Phys.* **24**, 106004 (2014).
35. P. Slavíček, D. Hollas, O. Svoboda, M. Ončk, ABIN, version 1.1 (2015).
36. G. Schmid, K. Schnorr, S. Augustin, S. Meister, H. Lindenblatt, F. Trost, Y. Liu, M. Braune, R. Treusch, C. D. Schröter, T. Pfeifer, R. Moshammer, Reaction microscope endstation at FLASH2. *J. Synchrotron Radiat.* **26**, 854–867 (2019).
37. S. Meister, H. Lindenblatt, F. Trost, K. Schnorr, S. Augustin, M. Braune, R. Treusch, T. Pfeifer, R. Moshammer, Atomic, molecular and cluster science with the reaction microscope endstation at FLASH2. *Appl. Sci.* **10**, 2953 (2020).
38. A. Senftleben, T. Pfeifer, K. Schnorr, K. Meyer, Y. H. Jiang, A. Rudenko, O. Herrwerth, L. Foucar, M. Kurka, K. U. Kühnel, M. Kübel, M. F. Kling, A. Yamada, K. Motomura, K. Ueda, R. Treusch, C. D. Schröter, R. Moshammer, J. Ullrich, Characterization of Extreme Ultra-Violet Free-Electron Laser Pulses by Autocorrelation, in *Multiphoton Processes and Attosecond Physics* K. Yamanouchi, M. Katsumi, Eds. (Springer, 2012), pp. 61–68.
39. J. C. Tully, Molecular dynamics with electronic transitions. *J. Chem. Phys.* **93**, 1061–1071 (1990).
40. T. Shiozaki, BAGEL: Brilliantly advanced general electronic-structure library. *Wiley Interdiscip. Rev. Comput. Mol. Sci.* **8**, e1331 (2018).
41. H.-J. Werner, P. J. Knowles, G. Knizia, F. R. Manby, M. Schütz, Molpro: A general-purpose quantum chemistry program package. *Wiley Interdiscip. Rev. Comput. Mol. Sci.* **2**, 242–253 (2012).
42. M. Ceriotti, G. Bussi, M. Parrinello, Langevin equation with colored noise for constant-temperature molecular dynamics simulations. *Phys. Rev. Lett.* **102**, 020601 (2009).
43. M. Ceriotti, G. Bussi, M. Parrinello, http://gle4md.org/.
44. A. D. Boese, J. M. Martin, Development of density functionals for thermochemical kinetics. *J. Chem. Phys.* **121**, 3405–3416 (2004).
45. G. W. T. M. J. Frisch H. B. Schlegel, G. E. Scuseria, M. A. Robb, J. R. Cheeseman, G. Scalmani, V. Barone, G. A. Petersson, H. Nakatsuji, X. Li, M. Caricato, A. Marenich, J. Bloino, B. G. Janesko, R. Gomperts, B. Mennucci, H. P. Hratchian, J. V. Ortiz, A. F. Izma, Gaussian 09 (2013).
46. K. Schnorr, "XUV pump-probe experiments on electron rearrangement and interatomic Coulombic decay in diatomic molecules," thesis, Ruprecht Karls University Heidelberg (2014).

47. S. Meister, "XUV free-electron laser experiments on weakly bound dimers: Construction of a water-dimer jet source and resonance-enhanced ICD in Ne_2," thesis, Ruprecht Karls University Heidelberg (2016).
48. F. Trost, "Pulse duration measurement at FLASH2 by intensity autocorrelation in neon and argon," thesis, Ruprecht Karls University Heidelberg (2017).
49. Y. H. Jiang, A. Rudenko, J. F. Pérez-Torres, L. Foucar, M. Kurka, K. U. Kühnel, M. Toppin, E. Plésiat, F. Morales, F. Martín, T. Jahnke, R. Dörner, J. L. Sanz-Vicario, J. van Tilborg, A. Belkacem, M. Schulz, K. Ueda, T. J. M. Zouros, S. Düsterer, R. Treusch, C. D. Schröter, M. Lezius, M. F. Kling, R. Moshammer, J. Ullrich, Investigating two-photon double ionization of D_2 by XUV-pump–XUV-probe experiments. *Phys. Rev. A* **81**, 051402 (2010).
50. K. Meyer, C. Ott, P. Raith, A. Kaldun, Y. Jiang, A. Senftleben, M. Kurka, R. Moshammer, J. Ullrich, T. Pfeifer, Noisy optical pulses enhance the temporal resolution of pump-probe spectroscopy. *Phys. Rev. Lett.* **108**, 098302 (2012).

Acknowledgments: We acknowledge DESY (Hamburg, Germany), a member of the Helmholtz Association HGF, for the provision of experimental facilities. Parts of this research were carried out at FLASH, and we would like to thank M. Braune and M. Kuhlmann for assistance in using the OPIS spectrometer and the beamline optics. Beamtime was allocated for proposal F-20150018. We are grateful for C. D. Schröter's support in setting up the Reaction Microscope. K.S. appreciates support through a Peter Paul Ewald fellowship from the Volkswagen Foundation. M.B. is a student of the International Max Planck Research School "Many-Particle Systems in Structured Environments." **Funding:** M.B. and P.S. thank the financial support of the Czech Science Foundation (grant no. 21-26601X, EXPRO project). **Author contributions:** Experiment: K.S., S.A., H.L., Y.L., S.M., R.M., T.P., G.S., R.T., and F.T. Theory: M.B. and P.S. Writing—original draft: K.S., M.B., and P.S. Writing—review and editing: all. **Competing interests:** The authors declare that they have no competing interests. **Data and materials availability:** All data needed to evaluate the conclusions in the paper are present in the paper and/or the Supplementary Material.

Submitted 27 January 2023
Accepted 8 June 2023
Published 12 July 2023
10.1126/sciadv.adg7864

Science Advances

Direct tracking of ultrafast proton transfer in water dimers

Kirsten Schnorr, Michal Belina, Sven Augustin, Hannes Lindenblatt, Yifan Liu, Severin Meister, Thomas Pfeifer, Georg Schmid, Rolf Treusch, Florian Trost, Petr Slaví#ek, and Robert Moshammer

Sci. Adv. **9** (28), eadg7864. DOI: 10.1126/sciadv.adg7864

Science Advances (ISSN 2375-2548) is published by the American Association for the Advancement of Science. 1200 New York Avenue NW, Washington, DC 20005. The title *Science Advances* is a registered trademark of AAAS.